ISSN 2063-5346

SYNTHESIS OF REDUCED GRAPHENE OXIDE SUPPORTED COBALT NICKEL OXIDE AND NEODYMIUM NICKEL OXIDE NANOCOMPOSITES FOR WASTEWATER TREATMENT

Mathivanan Nallathambi[1], Suganya Planisamy[2], Princy Jayakumar[3] and Krishnasamy Kuppusamy *

Article History: Received: 01.02.2023 **Revised:** 07.03.2023 **Accepted:** 10.04.2023

Abstract

Reduced graphene oxide based Cobalt Nickel oxide and Neodymium Nickel oxide nanocomposites were synthesized via facile hydrothermal method. The synthesized rGO/$CoNiO_2$ and rGO/$NdNiO_3$ nanocomposites were characterized by various analytical techniques such as XRD, FT-IR, SEM, XPS and UV-DRS. The crystalline size of rGO, NiO, $CoNiO_2$, $NdNiO_3$, rGO/$CoNiO_2$ and rGO/$NdNiO_3$ are found to be 19.8, 43.5, 46.3, 56.2, 50.4 and 64.5 nm respectively. Surface morphologies were examined by using SEM which revealed that agglomerated $CoNiO_2$ and flower shaped $NdNiO_3$ nanoparticles are distributed over the surface of rGO with a 2D sheet structure. The band gap was calculated using UV-DRS analysis and the Kubelka - Munk function plot scrutinized that band gap of rGO/$CoNiO_2$ and rGO/$NdNiO_3$ was found to be 3.0 and 2.7 eV respectively. Herein, we have employed methylene blue dye for the photocatalytic degradation purpose using rGO/$CoNiO_2$ and rGO/$NdNiO_3$ nanocomposites and are achieved up to 95% degradation property.

Keywords: Reduced graphene oxide, Nickel oxide, Hydrothermal, Methylene blue and Photocatalytic degradation.

Department of Chemistry, Annamalai University, Mail: krishnasamybala56@gmail.com.

DOI: 10.31838/ecb/2023.12.s1.127

Introduction

Environmental pollution has been a major problem encountered in recent years. The level of pollutants is increased day by day, causing severe and irreparable damage to the globe. Industrial effluents have been identified as the major source of water contamination. Photocatalytic degradation is an important wastewater treatment process that can eliminate harmful heavy organic contaminants[1]. Secondary effects of traditional wastewater treatment methods include the high cost of separation and the generation of secondary pollutants, associated with adsorption, clotting and membrane separation involving high operational costs[2]. The presence of graphene oxide is also enhanced the photocatalytic degradation property. $NdNiO_3$ is a rare earth metal oxide with wide-direct band gap. $NdNiO_3$ nanostructures have attracted great attention for potential applications and various fields such as photocatalytic performance, gas sensor, glucose sensor and solar cells[3,4]. Generally metal oxides have a better photocatalytic efficiency. rGO/$NdNiO_3$ acts as the best photocatalyst with high stability. As a result, the evolution of the new and efficient nanocomposite is progressively essential due to the environmentally beneficial product. In this study, rGO/$CoNiO_2$ and rGO/$NdNiO_3$ were used to estimate the degradation of methylene blue dye under sunlight irradiation and the observed results were studied and analyzed.

1. Experimental

1.1. Materials

In this study the required chemicals such as Graphite powder, Sodium nitrate, Sulphuric acid, Potassium permanganate, Nickel nitrate ($Ni(NO_3)_2$), Cobalt chloride hexahydrate ($CoCl_2.6H_2O$), Neodymium nitrate hexahydrate ($Nd(NO_3)_3{\cdot}6H_2O$), Oxalic acid and Hydrogen peroxide were in the analytical grade and used as such without any further purification.

1.2. Synthesis of Graphene Oxide

Graphene Oxide was synthesized by modified Hummer's method. 46 ml of H_2SO_4 and 1g of graphite powder and $NaNO_3$, were taken in the beaker and the solution was stirring for one hour at 500 rpm. 6g of $KMnO_4$ was added slowly and the solution was stirring half an hour in ice bath condition at 37°C for 30 minutes[6]. Further, 50 ml of water was added drop wise, and cooling the prearrangement in room temperature, then the arrangement was warming on 100 °C and 10ml of H_2O_2 was added for the formation of graphene oxide.

1.3. Synthesis of Reduced Graphene Oxide

400 mg of powdered Graphene oxide was dissolved in 20 ml of water and hydrazine hydrate (10 ml) was added and it used as a reducing agent to reduce the graphene oxide. The mixture was centrifuged at 4000 r/s for 40 minutes after being put on a magnetic stirrer for 30 minutes at 60 °C[7]. Then, the mixture was washed with ethanol and distilled water and dried for 24 hours at 120 °C.

1.4. Synthesis of Nickel Oxide

In a typical synthesis, Nickel oxide is synthesized via hydrothermal method. 2.33g of $Ni(NO_3)_2$ and 0.16 g of oxalic acid were dissolved in 70 ml of water. It was stirred continuously for half an hour at room temperature. The mixture was transferred into Teflon lined stainless steel autoclave and maintained at 120 °C for 12h. The product was washed with water and ethanol to remove unwanted impurities and dehydrated at 80 °C in air conditioning[8]. The resultant material was annealed at 400 °C for 5h in a muffle furnace.

1.5. Synthesis of $CoNiO_2$ and rGO/$CoNiO_2$ Nanocomposite

The $Ni(NO_3)_2.6H_2O$ (3.46g) and NaOH (0.7g) were dissolved in 60 ml of water. 1.9g of $CoCl_2.6H_2O$ was added slowly. The solution was stirred for half an hour at room temperature. The mixture was transferred to a Teflon-lined stainless-steel autoclave and maintained at 120 °C for 12 hours. The product was washed with water and ethanol, removed to remaining ions and dehydrated at 80 °C in air condition. The resulting powder was annealed at 450 °C for 5 hours in a muffle furnace. Finally, we are getting the product of $CoNiO_2$ nanocomposite. The powdered rGO added with the obtained $CoNiO_2$ to get rGO/$CoNiO_2$ nanocomposite.

1.6. Synthesis of $NdNiO_3$ and rGO/$NdNiO_3$ Nanocomposite

2.37g of $Ni(NO_3)_2.6H_2O$ and 0.3g of NaOH were dissolved in 60ml of water. 4.38g of $Nd(NO_3)_3{\cdot}6H_2O$ was added slowly. The solution was stirred at 30 min at room temperature. The obtained solution was transferred into Teflon autoclave and maintained at 20 °C at 12hrs. The product was washed with ethanol and water, removed to remaining charged ions and dehydrated at 80 °C in air. The resulting powder was annealed at 5hrs for 450 °C in a muffle furnace to get $NdNiO_3$. The above mentioned pathway was used to synthesize rGO/$NdNiO_3$ nanocomposite. The powdered rGO added with the obtained $NdNiO_3$ to get rGO/$NdNiO_3$ nanocomposite.

2.Characterization

2.1 XRD Analysis

The XRD patterns of the prepared samples after calcination at 450 °C and the observed diffraction peaks at 2θ values of reduced graphene oxide were found in the planes of (002) (100) and NiO nanoparticle were found in the planes of (311), (222), (220), (200), (111) and (004), respectively (**JCPDS Card No. 89-7390**)[13]. $CoNiO_2$ composite are ascribed to the reflection plane of (004), (200), (220), (311), (400), (422) and (511), it is well matched with **JCPDS Card No. 10-0188[14].** The composite of $NdNiO_3$ peaks appeared at planes of (002), (011), (012), (110), (103) and (511) and the plane values are well matched with **JCPDS Card No. 41-0344[15].** The reduced graphene oxide plane of (002) present in the composite spectrum indicates the graphene oxide percent in the composite. These phenomena indicate that the formation of rGO/$CoNiO_2$ and rGO/$NdNiO_3$ nanocomposite began at the calcination temperature of about 450 °C. Peaks are not detected in other phases, indicating the high purity of the products shown in **Fig.1**. The different parameters are calculated, such as the crystallite size of rGO/$CoNiO_2$ and rGO/$NdNiO_3$ nanocomposite using Debye–Scherrer formula (Equation 1) and the values are presented in **Table 1.**

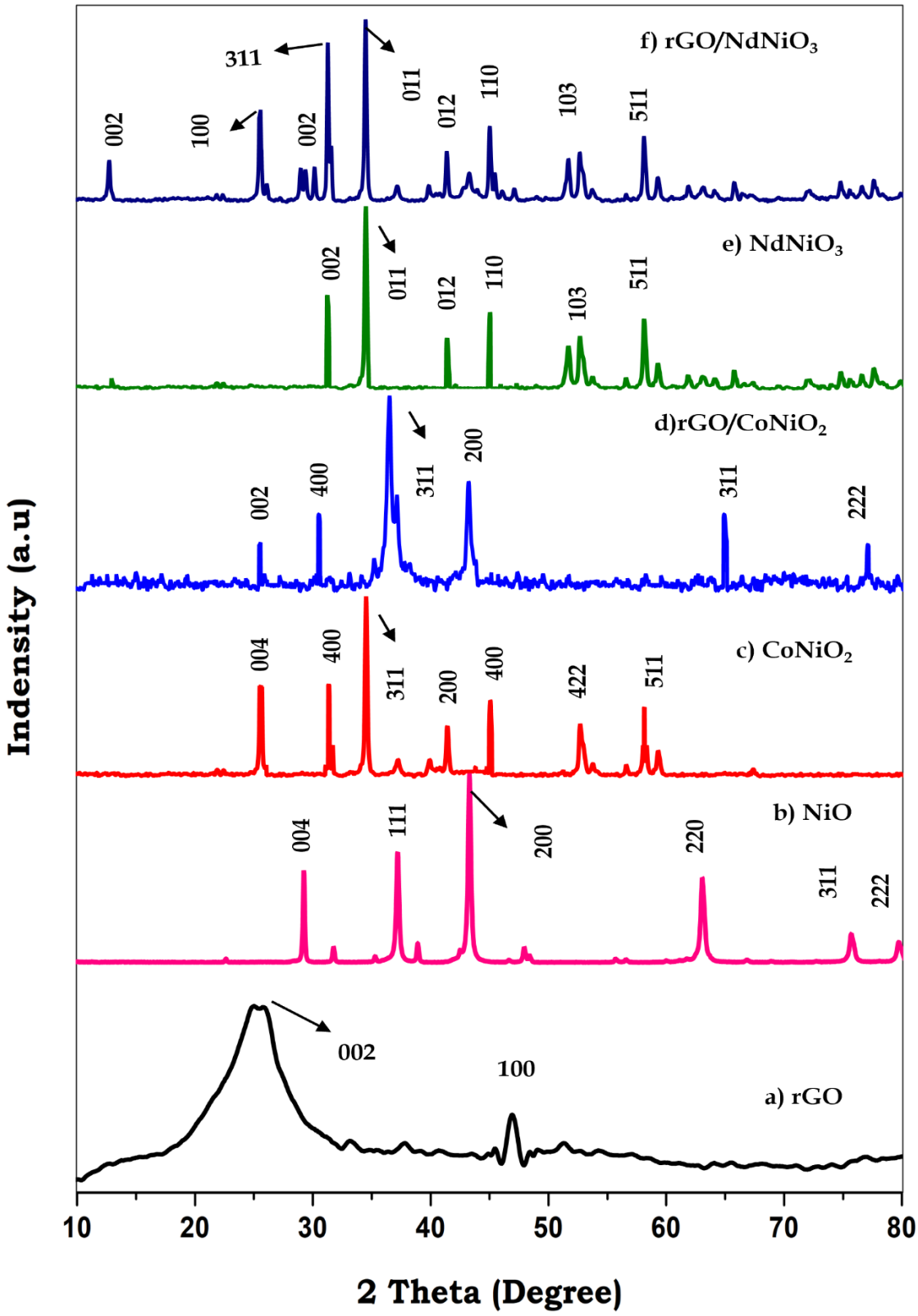

Fig.1 XRD spectra of (a) rGO (b) NiO (c) $CoNiO_2$ (d) rGO/$CoNiO_2$ (e) $NdNiO_3$ and (f) rGO/$NdNiO_3$

The crystalline size of the nanocomposites are calculated using the following Debye–Scherer's equation

$$\text{Crystalline size (D)} = \frac{0.9\lambda}{\beta \cos\theta} \quad \text{------ (1)}$$

Where λ is the wavelength (λ = 1.5406 Å (Cu Kα), β is the full width half maximum (FWHM) and θ is the diffraction angle.

Table.1. Crystalline size of (a)rGO (b)NiO (c)$CoNiO_2$ (d)rGO/$CoNiO_2$ (e)$NdNiO_3$ and (f)rGO/$NdNiO_3$

S.No	Sample	Crystaline Size(nm)
1.	rGO	19.8
2.	NiO	43.5
3.	$CoNiO_2$	46.3
4.	rGO/$CoNiO_2$	56.2
5.	$NdNiO_3$	50.4
6.	rGO/$NdNiO_3$	**64.5**

2.2 Functional group analysis

The FT-IR technique is a strong tool to analyze the different functional groups found in graphene oxide, including functional groups involving oxygen. FT-IR spectra of rGO shown in Fig.2a confirmed the well oxidation of the graphite and the peaks appeared at 599 and 607cm^{-1}. Fig.2b shows the vibration band observed at 3419 cm^{-1} is due to the stretching mode of H-O-H group of NiO. The stretching vibrations peak of 789 cm^{-1} due to the stretching mode of the Ni-O bond (Fig.2b). The $CoNiO_2$, M – O stretching vibrations appeared at 668 and 577 cm^{-1} and the characteristic bands at due to the H-O-H bond is appeared at 3400 cm^{-1} show in Fig.2c[16] and good agreement with the reported values. In $NdNiO_3$ composite the Ni-O band appeared at 541cm^{-1} and the H-O-H stretching vibrations peak appeared at 3512 cm^{-1} respectivly(Fig.2e). In the rGO/$CoNiO_2$ composite, the band at 576 and 661 cm^{-1} due the M-O-M streching vibration and H-O-H streching vibration apeared at 3400 cm^{-1}(Fig.2d) this co-existence may be significant, since it prevents the combination of charge carriers. In rGO/$NdNiO_3$ composite band appred at 541cm^{-1}, H-O-H streching vibration apeared at 3512 cm^{-1} and also induces a synergistic effect to enhance the catalytic activity of the nanocomposite.

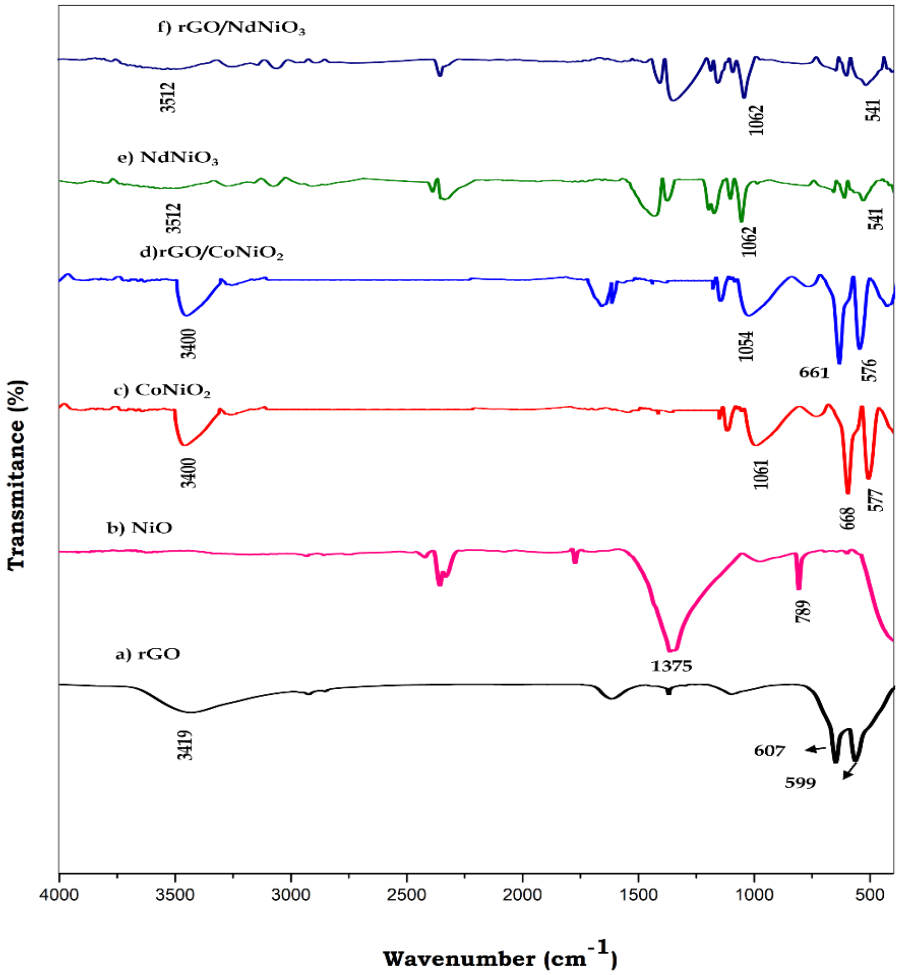

Fig. 2 FT-IR Spectra of (a)rGO (b)NiO (c)$CoNiO_2$ (d)rGO/$CoNiO_2$ (e)$NdNiO_3$ and (f)rGO/$NdNiO_3$

2.3 Morphology Analysis

The surface morphology of the as prepared rGO, NiO, $CoNiO_2$, $NdNiO_3$, rGO/$CoNiO_2$ and rGO/$NdNiO_3$ was analyzed using SEM micrographs and presented in Fig.3.a-f shows that the SEM images of rGO exhibited a sheet-like structure(Fig.3a). The NiO nanoparticle exhibited as an agglomerated. Further the surface morphology of $CoNiO_2$ nanoparticles are agglomerated shown in Fig.3c and the Fig.3d shows that exhibited flower like structure of $NdNiO_3$ nanoparticles[17]. Interestingly, rGO/$CoNiO_2$ nanocomposite displayed, the agglomerated $CoNiO_2$ nanoparticles are distributed in rGO surface in different directions (fig.3e) and the flower shaped $CoNiO_2$ nanoparticles are dispersed in smooth surface area of reduced graphene oxide(fig.3f).

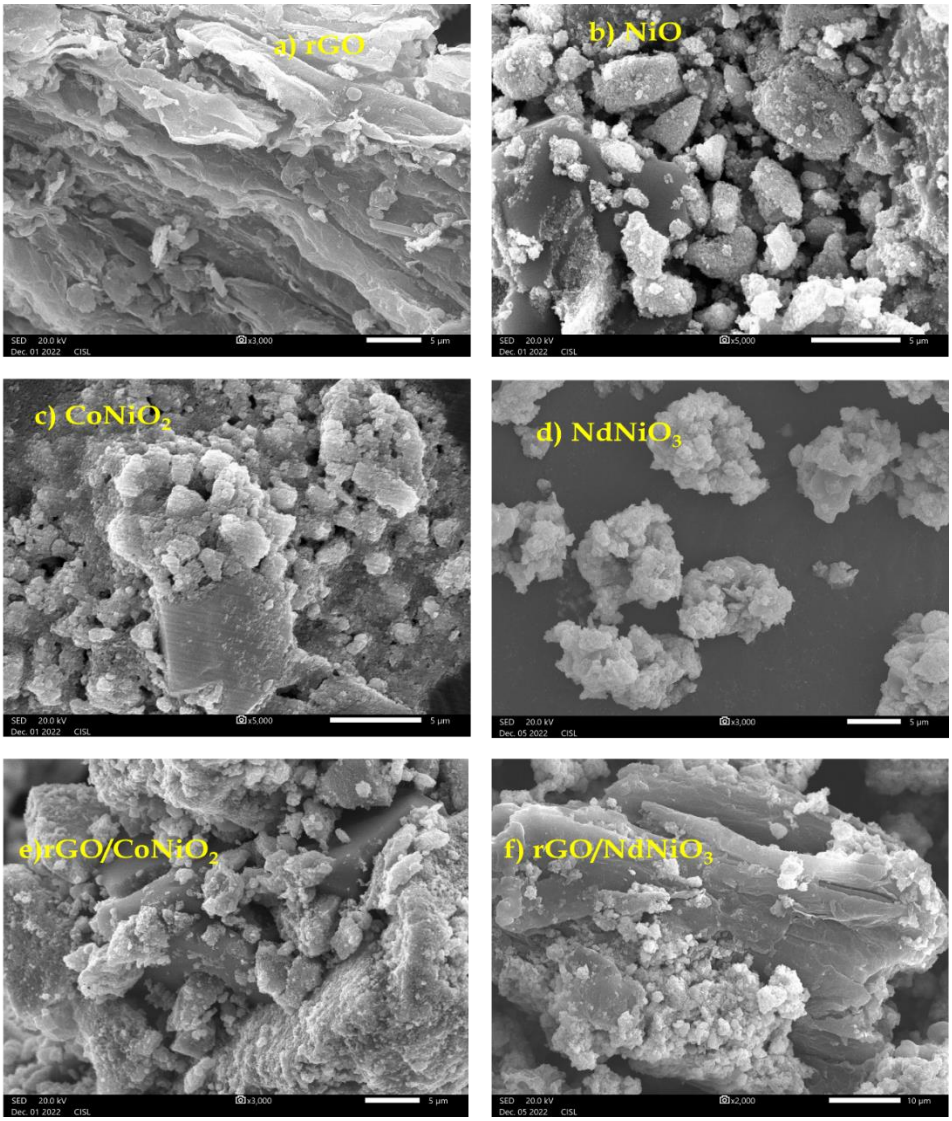

Fig.3 SEM analysis (a)rGO (b)NiO (c)$CoNiO_2$ (d)rGO/$CoNiO_2$ (e)$NdNiO_3$ and (f)rGO/$NdNiO_3$

2.4 UV - DRS Analysis

UV – diffuse reflectance spectroscopy of rGO/$CoNiO_3$ and rGO/$NdNiO_3$ nanocomposite are shown in Fig.4 and it is illustrated that rGO/$CoNiO_3$ and rGO/$NdNiO_3$ nanocomposite had significant UV absorption edge observed at 800nm. But the UV absorption of other samples shifted towards higher wavelength side. The changes in the absorption edges show the changes in the band structure. Further, the bandgap of samples is determined by Kubelka – Munk function (equation-2)[18].

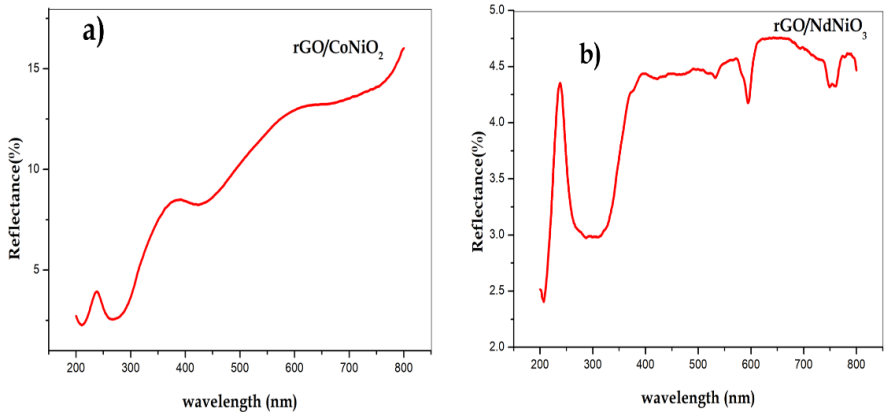

Fig.4 UV-DRS spectrum of (a) rGO/$CoNiO_2$ and (b) rGO/$NdNiO_3$

$$\alpha h\nu = A\,(h\nu - E_g)n \quad \text{------ (2)}$$

Where α is the absorption coefficient and hν is the incident photon energy. As shown in Fig.5, the bandgap energies are estimated from the intercept of the tangents. The band gap of prepared rGO/$CoNiO_2$ and rGO/$NdNiO_3$ nanocomposite were found to be 3.0 and 2.7 eV respectively. The presence of oxygen vacancies can create impurity level near the valance bond, the rGO/$NdNiO_3$ having lower band gap value and it is having more catalytic activity compared to the rGO/$CoNiO_2$ nanocomposite[19].

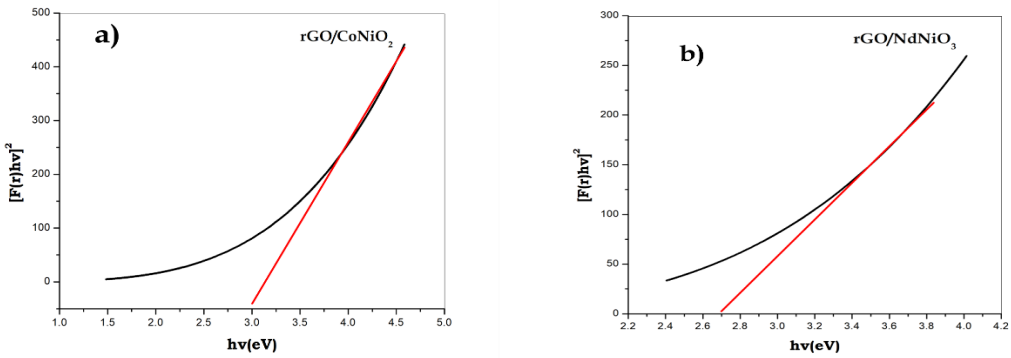

Fig.5 Tauc Plot of (a) rGO/$CoNiO_2$ and (b) rGO/NdNiO

XPS Analysis of rGO/$CoNiO_2$

The survey spectrum of rGO/$CoNiO_2$ shows in Fig. 6a, which exhibits Co, Ni, C and O elements without appearing any other impurities indicating the purity of the rGO/$CoNiO_2$ nanocomposite. The detailed study of high-resolution core level spectra of the Co, Ni, C and O elements are shows in the Fig.6b - 6e. Fig.6b shows the high resolution deconvoluted spectrum of Ni2p, it exhibits the two major peaks at 855.3 and 873.6 eV binding energies are corresponding to Ni2p $_{3/2}$ and Ni2p $_{1/2}$ respectively. Fig. 6c shows the deconvoluted spectrum of Co2p was exhibited at 781 eV and 796.2 eV corresponds to the Co2p $_{3/2}$ and Co2p $_{1/2}$ sates. The deconvoluted spectrum of the C1s state was shown in the Fig. 6d and it is observed at 285.2 eV. Moreover, the O1s state with the deconvoluted spectra of the rGO/$CoNiO_2$ nanocomposite was shown in Fig. 6e. This peak related to the oxygen containing functional groups was present in the reduced graphene oxide[19]. The peak at 531.4 eV corresponds to surface bonded water (H–O–H).

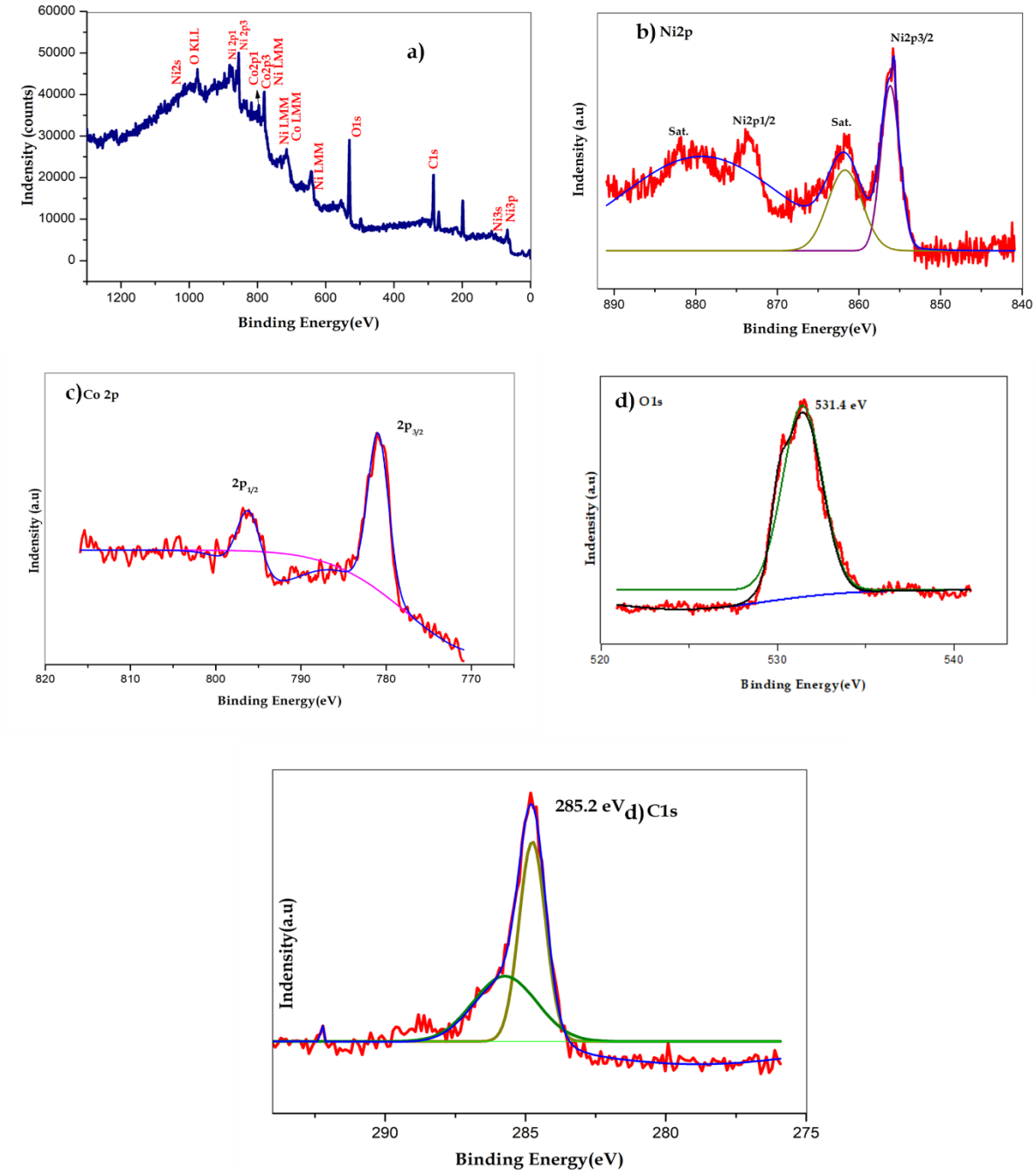

Fig.6 XPS spectra of rGO/$CoNiO_2$ nanocomposite (a) Survey spectrum, (b) Ni2p core spectrum, (c)Co2p core spectrum, (d) O1s core spectrum and (e) C1s core spectrum

XPS Analysis of rGO/$NdNiO_3$

The element oxidation states and surface binding of the prepared nanocomposites have been characterized through XPS analysis. Fig.7 shows the XPS spectra of rGO/$NdNiO_3$ nanocomposite. Fig.7a shows the survey spectrum of the rGO/$NdNiO_3$ nanocomposite, it shows the Nd2d, Ni2p, O1s and C1s binding energies alone presented in the rGO/$NdNiO_3$ nanocomposite. The detailed elemental composition of the rGO/$NdNiO_3$ nanocomposite was evaluated for the core level deconvoluted spectrum using Gaussian fitting. Fig. 7b - 7e shows the deconvoluted spectra of Nd2d, Ni2p, O1s

and C1s states. The deconvoluted spectrum of Nd3d was shown in Fig. 7b. From Fig. 7b, two binding energy levels are observed at 981.6 and 1003 eV corresponding to $Nd3d_{5/2}$ and $Nd3d_{3/2}$ in the Nd3d spectrum. These results reveal that the Ni species are in the +2-oxidation state. The core level Ni2p spectrum was shown in the Fig. 7c. In this Ni2p also shows binding energies of $Ni2p_{3/2}$ at 872.2 eV respectively. The core level spectrum Fig. 7d of O1s state appeared at 530.7 eV, which corresponds to the bonded oxygen either in $NdNiO_3$ lattice or in graphene[18]. The C1s peak is shown in Fig. 7e. Further, the peak intensities of oxygen (C-O) associated groups in the C1s peak at 284.3 eV are rather low, suggesting that a good degree of reduction has taken place where most of the oxygen functional groups have been removed. The significantly higher C=C peak intensity also shows the restoration of the disrupted sp^2 bonds during oxidation of graphite to GO.

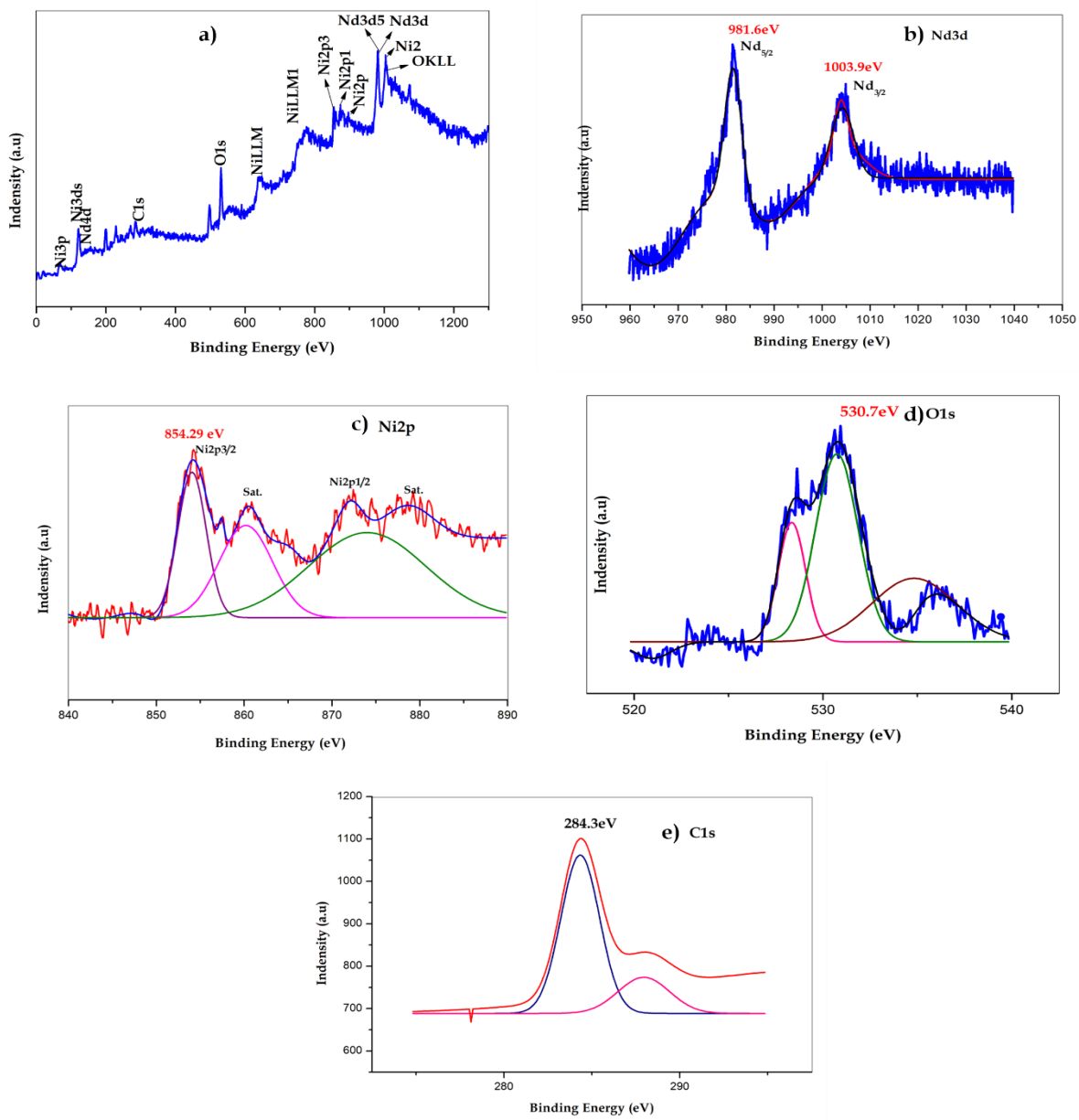

Fig.7 XPS spectra of rGO/$NdNiO_3$nanocomposite (a) Survey spectrum, (b) Nd3d core spectrum, (c)Ni2p core spectrum, (d) O1s core spectrum and (e) C1s core spectrum

3. Photocatalytic Activity

To find the degradation kinetics of methylene blue dye, 20mg of the catalyst was added to the dye solution and the system was kept in sunlight irradiation which was stirred magnetically. The system was observed manually and the degradation time was fixed as 60 minutes for methylene blue. When the catalyst was added into the dye solutions, the absorption peaks of the dye solution started to vanish and 5 ml of the samples were collected every 10 minutes for the UV analysis. The absorption curves (**Fig.8**), degradation efficiency (%) and absorbance plots (**Fig.9**) and kinetic analysis of photodegradation and degradation efficiency plots (**Fig.10**) which explained clearly about the degradation capability of the nanocatalysts[20]. The kinetic study for $rGO/CoNiO_2$ and $rGO/NdNiO_3$ nanocomposite (photocatalyst) for the degradation of Methylene blue were studied by using Langmuir – Hinshelwood kinetic model by using equation-3. The calculated rate constant of $rGO/CoNiO_2$ and $rGO/NdNiO_3$ nanocomposite for the photodegradation of methylene blue is 0.732 $x10^{-4}$ and 1.090 x 10^{-4} min^{-1}respectively.

$$\ln(C_o/C_t) = -kt \quad \ldots\ldots\ldots \quad (3)$$

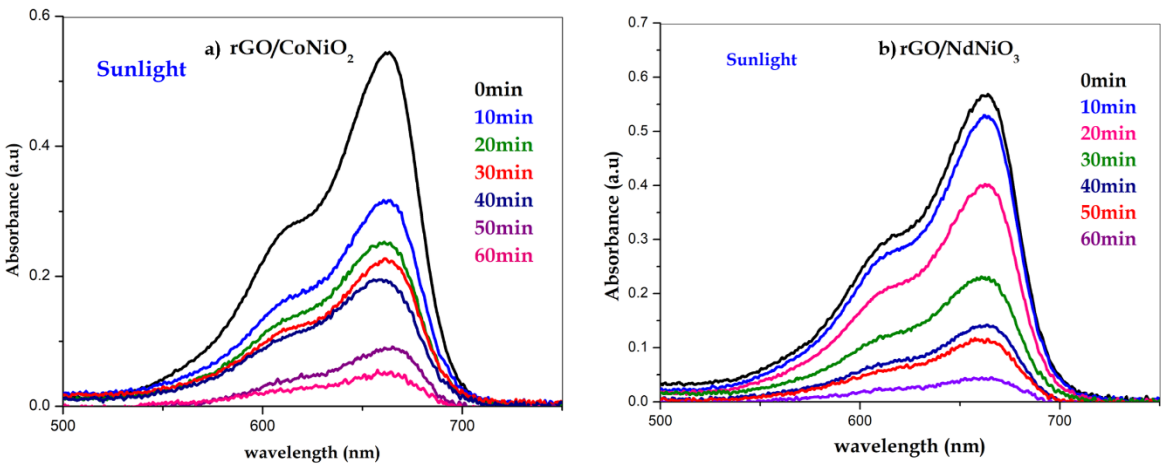

Fig.8 UV-Visible spectra for the photocatalytic degradation of methylene blue dye by $rGO/CoNiO_2$ and $rGO/NdNiO_3$ nanocomposite under sunlight irradiation.

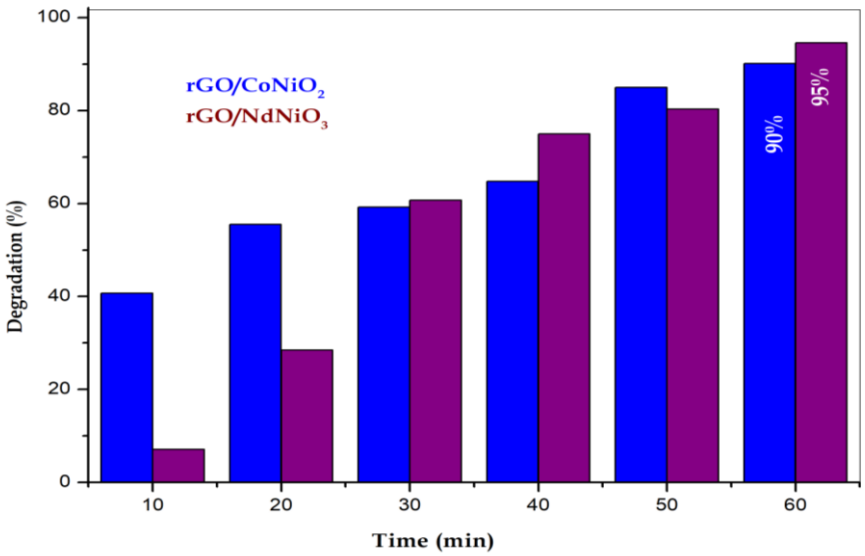

Fig. 9 Degradation efficiency(%) of $rGO/CoNiO_2$ and $rGO/NdNiO_3$ nanocomposite.

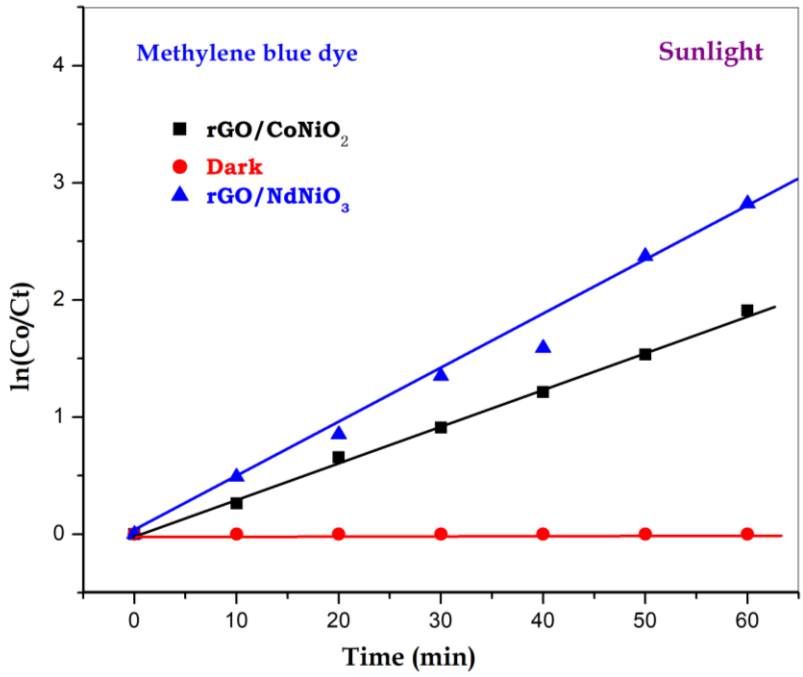

Fig.10 Pseudo-first-order plot of Methylene blue dye catalyzed by rGO/$CoNiO_2$ and rGO/$NdNiO_3$ nanocomposite.

3.1 Mechanism of Photocatalytic Activity

The mechanistic aspects of this photodegradation are as follows. The dye molecules can migrate to the catalyst surface, where they can undergo a redox reaction with other species present on the surface. Usually, electron-hole can react easily with surface-bound H_2O to produce $OH^{\bullet}$ radicals whereas conduction band electrons can react with O_2 to produce superoxide radical anion of oxygen[21].

This reaction prevents the combination of the electron and the hole which are produced in the first step. These $OH^{\bullet}$ and $O_2^{\bullet -}$ can then react with the dye molecule to form other species and are thus responsible for the decolorization of the dye[22]. This catalytic degradation process is used for treating toxic industrial effluent and making a pollution-free environment.

$$\text{Photocatalyst} + h\upsilon \longrightarrow h^{+}_{VB} + e^{-}_{CB}$$

$$h^{+}_{VB} + e^{-}_{CB} \longrightarrow \text{Energy (heat)}$$

$$H_2O + h^{+}_{VB} \longrightarrow OH^{\bullet} + H^{+}$$

$$O_2 + e^{-}_{CB} \longrightarrow O_2^{\bullet -}$$

$$OH^{\bullet} + \text{Pollutant} \longrightarrow H_2O + CO_2$$

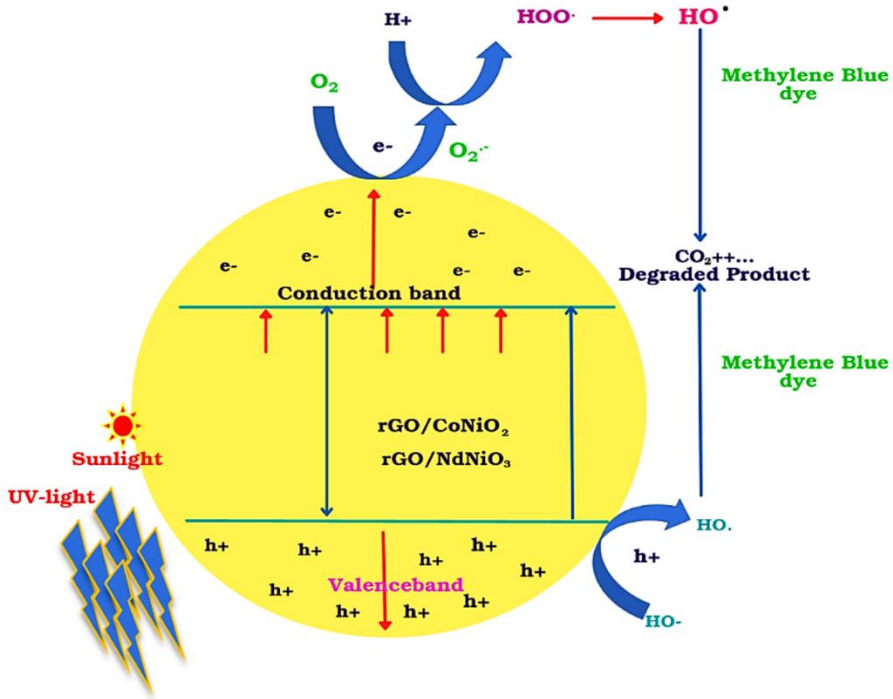

Fig. 11 Photocatalytic mechanism of rGO/$CoNiO_2$ and rGO/$NdNiO_3$ nanocomposite.

Conclusion:

The hydrothermal approach was employed to synthesize the nanomaterials viz., rGO, NiO, $CoNiO_2$, $NdNiO_3$, rGO/$CoNiO_2$ and rGO/$NdNiO_3$. The prepared materials were calcined at 450°C for 6 hours, producing NiO, $CoNiO_2$, $NdNiO_3$, rGO/$CoNiO_2$ and rGO/$NdNiO_3$ nanomaterials with a crystalline size of 19.8, 43.5, 46.3, 56.2, 50.4 and 64.5 nm. Surface morphology was examined by using SEM which revealed that agglomerated $CoNiO_2$ and flower shaped $NdNiO_3$ nanoparticles are distributed over the surface of rGO with a 2D sheet structure. Kubelka - Munk function plot scrutinized the band gap of rGO/$CoNiO_2$ and rGO/$NdNiO_3$ 3.0 and 2.7 eV, respectively. The photocatalytic performance of the synthesized rGO/$CoNiO_2$ and rGO/$NdNiO_3$ against methylene blue dye was evaluated by sunlight irradiation. rGO/$NdNiO_3$ nanocomposite having a high degradation property (95%) compared to rGO/$CoNiO_2$ (90%) nanocomposite.

Reference:

1. Haanappel, V. A. C., Lalanne, C., Mai, A., & Tietz, F. (2009). Characterization of anode-supported solid oxide fuel cells with Nd_2NiO_4 cathodes. *Journal of Fuel Cell Science and Technology*, *6*(4).
2. Rodríguez-González, V., Terashima, C., & Fujishima, A. (2019). Applications of photocatalytic titanium dioxide-based nanomaterials in sustainable agriculture. *Journal of Photochemistry and Photobiology C: Photochemistry Reviews*, *40*, 49-67.
3. Narayanan, D. P., Gopalakrishnan, A., Yaakob, Z., Sugunan, S., & Narayanan, B. N. (2020). A facile synthesis of clay–graphene oxide nanocomposite catalysts for solvent free multicomponent Biginelli reaction. *Arabian Journal of Chemistry*, *13*(1), 318-334.

4. Adetayo, A., & Runsewe, D. (2019). Synthesis and fabrication of graphene and graphene oxide: A review. *Open Journal of Composite Materials*, *9*(02), 207.
5. Shen, H., Wang, Y. Z., Liu, G., Li, L., Xia, R., Luo, B., ... & Yong, Y. C. (2020). A whole-cell inorganic-biohybrid system integrated by reduced graphene oxide for boosting solar hydrogen production. *Acs Catalysis*, *10*(22), 13290-13295.
6. Luo, L., Yang, M., & Chen, G. (2020). Continuous synthesis of reduced graphene oxide-supported bimetallic NPs in liquid–liquid segmented flow. *Industrial & Engineering Chemistry Research*, *59*(17), 8456-8468.
7. Jana, A., Scheer, E., & Polarz, S. (2017). Synthesis of graphene–transition metal oxide hybrid nanoparticles and their application in various fields. *Beilstein Journal of Nanotechnology*, *8*(1), 688-714.
8. Dideikin, A. T., & Vul, A. Y. (2019). Graphene oxide and derivatives: the place in graphene family. *Frontiers in Physics*, *6*, 149.
9. Zakaria, M. B., Zheng, D., Apfel, U. P., Nagata, T., Kenawy, E. R. S., & Lin, J. (2020). Dual-heteroatom-doped reduced graphene oxide sheets conjoined CoNi-based carbide and sulfide nanoparticles for efficient oxygen evolution reaction. *ACS Applied Materials & Interfaces*, *12*(36), 40186-40193.
10. Kawahara, A., & Ishihara, T. (2010). Oxygen permeation property in Nd Deficient Nd_2NiO_4 mixed oxide doped with Cu and Ga. *Electrochemical and Solid-State Letters*, *13*(7), B76.
11. Buttrey, D. J., & Honig, J. M. (1988). Influence of nonstoichiometry on the magnetic properties of Pr_2NiO_4 and Nd_2NiO_4. *Journal of Solid-State Chemistry*, *72*(1), 38-41.
12. Puche, R. S., Fernández, F., Carvajal, J. R., & Martinez, J. L. (1989). Magnetic and X-ray diffraction characterization of stoichiometric Pr_2NiO_4 and Nd_2NiO_4 oxides. *Solid State Communications*, *72*(3), 273-277.
13. Castro, M., & Burriel, R. (1995). Phase transitions and crystal-field levels in Nd_2NiO_4. *Thermochimica Acta*, *269*, 523-535.
14. Rodríguez-Carvajal, J., Fernández-Díaz, M. T., Martínez, J. L., Fernández, F., & Saez-Puche, R. (1990). Structural phase transitions and three-dimensional magnetic ordering in the Nd_2NiO_4 Oxide. *Europhysics Letters*, *11*(3), 261.
15. Batlle, X., Martinez, B., Obradors, X., Pernet, M., Vallet, M., Gonzalez-Calvet, J., & Alonso, J. (1992). Study of the magnetic properties of Nd_2NiO_4. *Journal of Magnetism and Magnetic Materials*, *104*, 918-920.
16. Chefi, S., Kahlaoui, M., Inoubli, A., Madani, A., & Hammou, A. (2013). Ageing effect on electrical properties of the oxyapatite/Nd_2NiO_4 interface. *Ceramics International*, *39*(4), 4507-4512.
17. Mauvy, F., Lalanne, C., Bassat, J. M., Grenier, J. C., Brisse, A., Sauvet, A. L., ... & Fouletier, J. (2009). Electrochemical study of the $Nd_{1.95}NiO_{4+\delta}$/oxide electrolyte interface. *Solid State Ionics*, *180*(20-22), 1183-1189.
18. Sun, L. P., Li, Q., Zhao, H., Huo, L. H., & Grenier, J. C. (2008). Preparation and electrochemical properties of Sr-doped Nd_2NiO_4 cathode materials for intermediate-temperature solid oxide fuel cells. *Journal of Power Sources*, *183*(1), 43-48.

19. Yang, M., Bucher, E., & Sitte, W. (2011). Effects of chromium poisoning on the long-term oxygen exchange kinetics of the solid oxide fuel cell cathode materials La0. 6Sr$_0$. 4CoO_3 and Nd_2NiO_4. *Journal of Power Sources*, *196*(17), 7313-7317.
20. Murata, A., Uchikoshi, T., & Matsuda, M. (2015). Fabrication and characterization of oriented Nd_2NiO_4 bulk and cathode for low-temperature operating solid oxide fuel cell. *Journal of Power Sources*, *293*, 95-100.
21. Bhavaraju, S., DiCarlo, J. F., Scarfe, D. P., Yazdi, I., & Jacobson, A. J. (1994). Electrochemical Intercalation of Oxygen in Nd_2NiO_4. *Chemistry of Materials*, 6(11), 2172-2176.
22. Pikalova, E.Y., Sadykov, V.A., Filonova, E.A., Eremeev, N.F., Sadovskaya, E.M., Pikalov, S.M., Bogdanovich, N.M., Lyagaeva, J.G., Kolchugin, A.A., Ishchenko, A.V., Goncharov, V.B., Structure, oxygen transport properties and electrode performance of Ca-substituted Nd_2NiO_4. *Solid State Ionics*. 2019 Jul 1; 335:53-60.